TA17 design of wideband optics I

Prepared By:
Michel Doucet

INO
2740 Einstein Street
Québec, Québec G1P 4S4

PWGSC Contract Number: W7701-091881

Contract Scientific Authority:
Mr. Philips Laou, Ph.D. 418-844-4000 x4218

Contract Report
DRDC-RDDC-2014-C201
March 2014

REPORT

TA17 DESIGN OF WIDEBAND OPTICS I

INO 101525-17DW R N/A

Presented to:

Mr. Philips Laou
DRDC Valcartier
2459 Boul de la Bravoure
Quebec (QC) G3J 1X5

Prepared by:
Michel Doucet

Presented by:

Geneviève Anctil
Project Manager

Approved by:

Alain Bergeron
Program Manager, Defense and Security

INO

March 2014

INO • 2740 Einstein Street, Québec (Québec) Canada G1P 4S4

This page is intentionally left blank

TABLE OF CONTENTS

TA17-DESIGN OF WIDEBAND OPTICS I

1 INTRODUCTION

The TA17 is part of the contract W7701-091881/001/QCL. The task consists in a design study on imaging optics for a wide waveband cooled sensor array over the range of 1-4.2 µm for the new Kinglet wideband sensor from SCD.

2 HYPOTHESIS, DESCRIPTION OF THE DESIRED OPTICS

The study concerns imaging systems operating over a large waveband that includes the shortwave infrared (SWIR) and a part of the midwave infrared (MWIR). More specifically, the study concerns two different types of imaging systems with similar characteristics except for their field-of-views (FOV) and corresponding focal lengths.

Table 2.1 gathers the main characteristics wanted for the new imaging optics.

Table 2.1- Basic characteristics wanted for the imaging optics

Characteristic	Value	Comments
Field-of-view (FOV)	8x10° (WFOV) 4x5° (NFOV)	Corresponds to the total FOV in the two perpendicular principal axis of the sensor array.
Image size	7.68 x 9.6 mm	Corresponds to the SCD Kinglet detector format, i.e. 512 x 640 square pixels with 15 µm pitch.
F/#	4 – 5.5	
Focal length	55 mm (WFOV) 110 mm (NFOV)	This parameter is slave to the FOV and the image size. The amount of distortion has also an impact on this parameter.
Stop	External	The stop is located inside the sensor cooled Dewar at 19.6 mm in front of the sensitive surface of the sensor array. No vignetting is allowed since the sensor should not see any of the mechanical parts of the optical system.
Focus range	25 m to ∞	This involves an axial displacement range of about 120 µm and 485 µm respectively for the WFOV and NFOV systems.
Spectral range	1-4.2 µm	This is not a usual waveband.
Operational thermal range	-40 to 50°C	20°C is the nominal temperature. Degradations of the optimal performances are expected for temperature different from the nominal. The degradation should be controlled within the operational range of temperatures.

3 DESIGN OPTIONS

The design of a wide-band optics for the SWIR-MWIR bands encompasses various challenges. One of the questions arising from the specifications concerns the correction of the chromatism inherent to a wideband design. The question should be put into the perspective of a limited choice of materials with reasonable internal transmission over the entire 1-4.2 µm spectral band. Obviously, the control of the chromatism is evacuated if the choice of using only reflective elements is made. However in the context of the actual imaging systems, a refractive approach presents many advantages over a reflective counterpart in terms of the simplicity, compactness and mass. The reflective approach involves off-axis unobscured configurations (OUC) because of the difficulties associated with centered reflective systems for the control of parasitic light emitted by the mechanical parts surrounding the optical elements (support or baffles). The difficulty of placing the stop outside an off-axis unobscured reflective system is also a drawback for the reflective approach. For all these reasons, the priority was put on the refractive approach and efforts on the identification of materials have been put on the generation of a catalog that includes commercially available materials with interesting transmission characteristics in the desired waveband.

4 OPTICAL MATERIALS

The specification for the spectral waveband 1-4.2 µm comes from the recent availability of new wideband sensors such as the *Kinglet* designed by *SemiConductor Devices* (SCD) of Israel. The existence of *SuperBand* lens series from *StingRay* [4] seems to indicate that there exist materials allowing the creation of refractive optics that can operate efficiently in the wide 1-4.2 µm spectral waveband. However, it is not known if *StingRay* devices use exclusive proprietary materials not available on a commercial basis.

INO has made a survey for materials transmitting in the 1-4.2 µm spectral waveband. Materials with significant failure risks related to harsh environment were discarded from the catalog since military applications require ruggedized equipment. Table 4.1 shows the lists of the materials included in the catalog specifically created for the study. The list includes both crystal and chalcogenide glass but no common silicate glass since it seems that none of them is transmitting up to 4 µm. In the case of the crystal, only those crystallizing in the cubic lattice system are included since they exhibit isotropic optical properties. The only one exception to this selection rule is sapphire since its birefringence is very low and does not cause important problem in low numerical aperture optical systems. The chalcogenide glasses are compounds formed predominantly from one or more of the chalcogenide elements, mainly sulphur, selenium and tellurium [1]. The catalog includes chalcogenide glasses produced by Schott and Amorphous Material Inc. in United States, but such materials are produced by other manufacturers. The chalcogenide glasses produced by Umicore (GASIR, France) and Lightpath (Black Diamond, USA) have not been included in the catalog because of lack of data on their index of refraction. A non-exhaustive list of manufacturers for each of the material is given in table 4.1. They are identified by their number as listed in table 4.2 which contained the addresses and web site coordinates of the main material manufacturers.

Table 4.1- Lists of optical materials included in the catalog.

Material	n @ 3 mm	Dispersion V	TCE (10^{-6}/°C)	Type	Manufacturers
AMTIR1	2.5190567	16.4547117	12	Chalcogenide	1
BaF_2	1.46115171	32.9913221	18.4	Crystal, cubic	2, 3, 5, 7
CaF_2	1.41785035	18.0049238	18.9	Crystal, cubic	2, 3, 5, 7
ZnS clear	2.25767563	29.5419241	6.3	Crystal, cubic	3, 4, 5, 6
IRG22[1]	2.51808931	17.8767941	12.1	Chalcogenide	4
IRG23[1]	2.81109614	10.6086303	13.4	Chalcogenide	4
IRG24[1]	2.62738771	15.657436	20.4	Chalcogenide	4
IRG25[1]	2.62776854	15.0716993	14.0	Chalcogenide	4
IRG26[1]	2.80149219	13.0120097	20.8	Chalcogenide	4
SAPPHIRE	1.71224426	7.18670178	6.63	Crystal, tetragon	4, 5
ZnSe	2.43757888	25.1569556	7.1	Crystal, cubic	3, 5

1- Data derived directly or indirectly from Schott

2- See references [3,8,9,10]

Table 4.2-List of material manufacturers.

#	Manufacturer name	Address	Web
1	Amorphous Materials Inc.	3130 Benton St Garland, TX 75042	www.amorphousmaterials.com/
2	Hellma Materials GmbH	Moritz-von-Rohr-Straße 1 07745 Jena, Germany	www.hellma-materials.com
3	Impex HighTech GmbH	Hovesaatstr. 6, 48432 Rheine Germany	www.impex-hightech.de
4	Schott, North America	400 York Avenue Duryea, 18642, USA	www.us.schott.com
5	MaTecK GmbH	Im Langenbroich 20 Juelich 52428 Germany	www.mateck.com
6	Dow Chimical	Philadelphia, PA USA	www.dow.com/
7	Corning Incorporated	24 E. Brookfield Road, PO Box 189, Brookfield Road, MA 01535	www.corning.com/specialtymaterials

The catalog presents some risks in term of the supply of the chalcogenide glasses. The IRGxx chalcogenide glasses was originally developed and produced by Vitron in Germany, but the production has been transferred to the Schott factory located in the United States [6]. It is not sure that the procurement of the IRGxx or AMTIR materials can be achieved outside the ITAR legislations and its constraints. However, the IRGxx equivalents may still be available from Vitron in Germany.

5 OPTICAL CONFIGURATIONS

Various configurations have been considered during the optical design process. The development of most of them have been stopped at their early stage of optimization. Only few of the envisioned configurations have been pushed further in the development process. The most interesting configurations obtained during the design exploration are presented in this section. The designs for the WFOV are presented first; they consist only in refractive systems. The NFOV designs include mainly refractive systems but at least one reflective design was developed. The WFOV and NFOV designs are presented in two distinct sub-sections.

For all designs done in this study, the SCD Kinglet was considered for the optical configuration of the Dewar. The Dewar of the Kinglet device is closed by a 1 mm thick window made of Cleartran. There is a gap of 1 mm between the window back surface and the cold stop which is located 19.6 mm in front of the sensitive surface of the pixel array. The standard Kinglet package includes a spectral filter which is fixed to the cold stop. The sapphire substrate of this filter is 0.5 mm thick. The spectral filter was not included in most of the designs presented in this report since DRDC plane to purchase the Kinglet sensor without the filter.

5.1 WFOV CONFIGURATIONS

The WFOV configurations have relatively small focal length of about 55 mm. Configuration with 3, 4 and 5 lenses were explored either with and without aspheric surfaces. In most cases, control of the chromatic aberrations is an important problem.

Figure 5.1 shows four of the most interesting WFOV configurations with few rays. Relative dimensions have been approximately preserved to show the size difference between the designs. Configurations A and B both consist of only three lenses while configurations C and D include respectively four and five lenses. Configuration A, C and D consist of spherical surfaces only while configuration B has one aspheric surface. Table 5.1 gathers the main characteristics of the optical configurations appearing in figure 5.1.

Table 5.1-Main characteristics of the WFOV configurations.

	Units	A	B	C	D
Number of lenses		3	3	4	5
Number of aspheric surface		0	1	0	0
Total length first surface/Dewar window	mm	36	36	39	35
Approximate mass[1]	g	36	37	43	35
Max lens diameter[1]	mm	29.8	30	30.05	29.25
Distance last surface/Dewar window	mm	12.2	11.9	9.1	8.3

1-Tight diameter. Just the diameter to allow all the rays to be transmitted. No extra space for the mechanical supports.

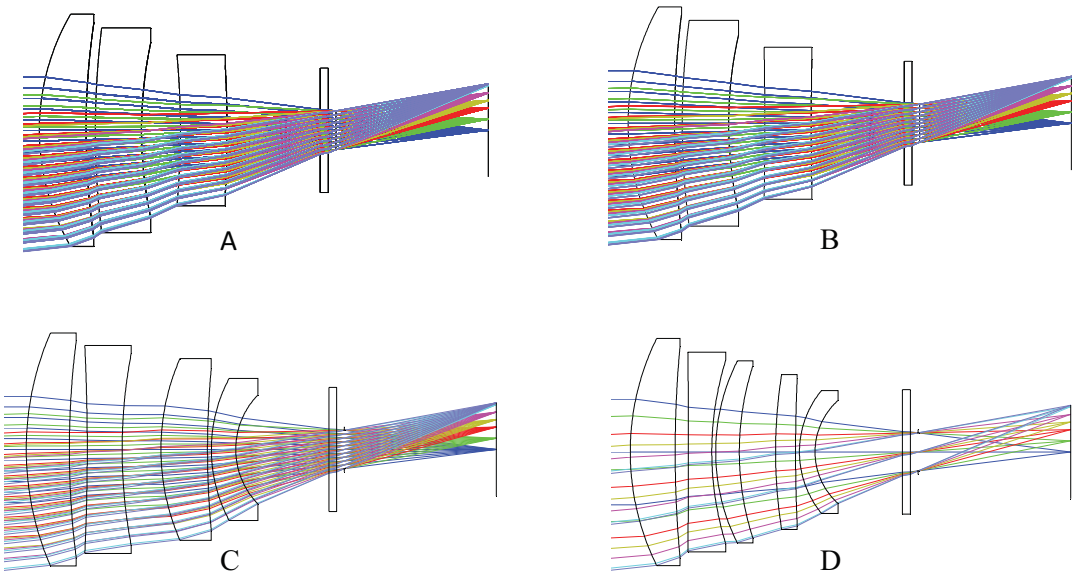

Figure 5.1- Most interesting configurations for the WFOV system.

Tables 5.2 to 5.5 give draft of the optical prescriptions respectively for the configurations A, B, C and D. In the case of configuration B which includes an aspheric surface, the aspheric coefficients have been omitted in the main description (Even Asphere, EVENASPH) to avoid overloading the table but is included at the bottom of the table. In all cases, the last 4 surfaces correspond to the Dewar optical layout.

Table 5.2- Draft of the optical prescription for the configuration A

#	Type	Radius	Thickness	Glass	Diameter
2	STANDARD	29.724522	6.000	CLEARTRAN	29.875
3	STANDARD	95.006250	1.207		27.725
4	STANDARD	107.564942	5.936	IRG26	26.339
5	STANDARD	53.992436	5.000		22.568
6	BIRE__IN	-105.79683	6.000	SAPPHIRE	19.460
7	BIRE_OUT	-143.81513	12.000		16.720
8	STANDARD	Inf	1.000	CLEARTRAN	16.000
9	STANDARD	Inf	1.000		16.000
10	STANDARD	Inf	19.600		4.941
11	STANDARD	Inf	0.000		12.010

Table 5.3- Draft of the optical prescription for the configuration B

#	Type	Radius	Thickness	Glass	Diameter
2	STANDARD	30.893423	6.000	CLEARTRAN	30.056
3	STANDARD	110.457941	0.992		27.981
4	EVENASPH	97.166756	6.000	IRG26	26.589
5	STANDARD	51.696286	4.659		22.688
6	BIRE__IN	-554.232099	6.000	SAPPHIRE	19.620
7	BIRE_OUT	454.743855	12.000		16.440
8	STANDARD	Inf	1.000	CLEARTRAN	16.000
9	STANDARD	Inf	1.000		16.000
10	STANDARD	Inf	19.600		4.893
11	STANDARD	Inf	0.000		12.121

Surface # 4, aspheric parameters	Units	Values
Conic constant		-3.753981
Aspheric coefficient, r^4	$1/mm^3$	-3.7550206E-07
Aspheric coefficient, r^6	$1/mm^5$	3.6890531E-09
Aspheric coefficient, r^8	$1/mm^7$	-9.2699916E-12

Table 5.4- Draft of the optical prescription for the configuration C

#	Type	Radius	Thickness	Glass	Diameter
2	STANDARD	37.708305	5.555	ZNSE	30.053
3	STANDARD	111.443273	2.305		28.085
4	STANDARD	-284.140911	4.498	IRG25	26.791
5	STANDARD	65.893619	5.000		24.841
6	STANDARD	29.135386	6.000	CLEARTRAN	23.406
7	STANDARD	111.761067	0.500		21.057
8	STANDARD	19.433635	3.142	CAF2	18.337
9	STANDARD	10.069106	12.000		14.076
10	STANDARD	Inf	1.000	CLEARTRAN	16.000
11	STANDARD	Inf	1.000		16.000
12	STANDARD	Inf	19.600		4.934
13	STANDARD	Inf	0.000		12.063

Table 5.5- Draft of the optical prescription for the configuration D

#	Type	Radius	Thickness	Glass	Diameter
2	STANDARD	33.127050	5.773	ZNSE	29.233
3	STANDARD	148.695792	1.709		27.266
4	STANDARD	-993.430031	3.000	IRG26	25.694
5	STANDARD	39.778170	0.500		23.588
6	STANDARD	26.028750	3.037	AMTIR1	23.434
7	STANDARD	35.994951	4.661		22.171
8	STANDARD	63.796117	2.570	AMTIR1	19.924
9	STANDARD	213.672884	0.500		19.076
10	STANDARD	12.435123	2.000	CAF2	15.827
11	STANDARD	8.908510	11.250		13.274
12	STANDARD	Inf	1.000	CLEARTRAN	16.000
13	STANDARD	Inf	1.000		16.000
14	STANDARD	Inf	19.600		4.890
15	STANDARD	Inf	0.000		12.053

5.2 NFOV CONFIGURATIONS

The focal length corresponding to the NFOV is relatively long, about 110 mm and this involves significantly heavier optical systems in comparison to the WFOV systems. For a given focal ratio, the mass does not increase linearly with the focal length but more as the square of the focal length. The NFOV refractive configurations obtained in this study are typically more than 5 times heavier than WFOV counterparts. A mass of 320 g for the optical material was considered too large for the envisioned applications. A reflective design has been sketched but it rapidly becomes evident that it would be difficult to obtain compact configurations with the reflective approach. Hence, NFOV configurations were not considered interesting and their development were not pushed farther than the early exploratory stage. For those reasons, the NFOV configurations are presented briefly.

Figure 5.2 presents the most interesting refractive configuration on its left side and the reflective design on the right. Note that the schemas are not to scale and that the reflective design is significantly larger than the refractive counterpart. The refractive configuration consists of spherical surfaces while the reflective configuration consists of off-axis aspheric surfaces and is thus more complex. Table 5.6 gathers the main characteristics of the two optical configurations and table 5.7 gives a draft optical prescription of the refractive configuration. The optical prescription of the reflective system has been omitted for brevity and also because of the complexity of the configuration and the complexity to present it in a compact format.

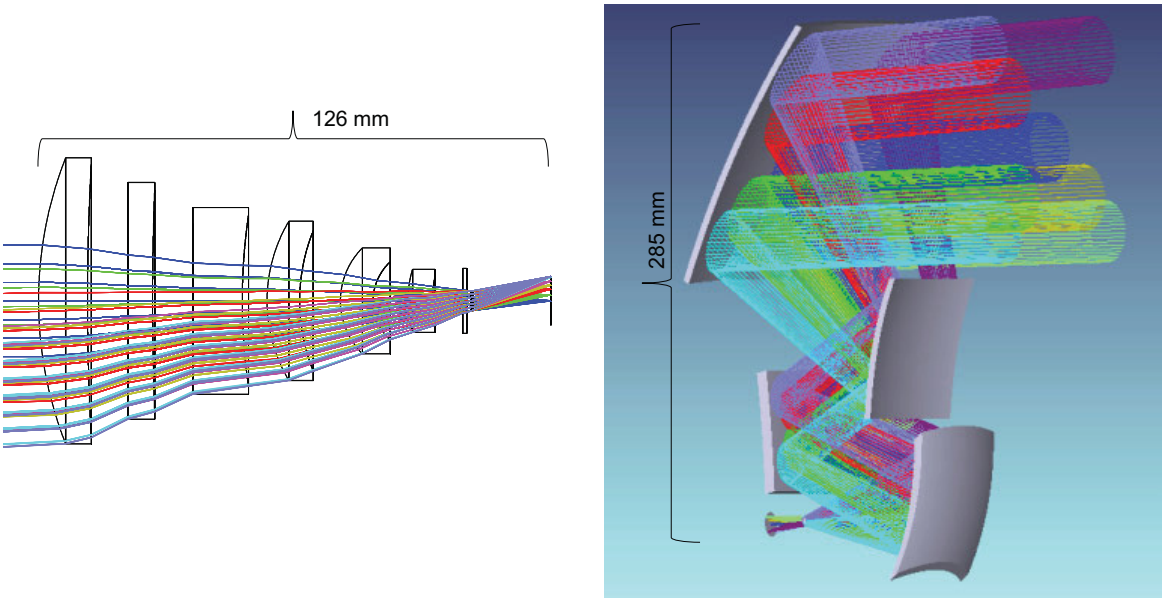

Figure 5.2- NFOV exploratory designs, the refractive configuration on left and the entirely reflective on right.

Table 5.6-Main characteristics of the NFOV configurations.

	Units	Refractive	Reflective
Number of optical elements		6	4
Number of aspheric surface		0	4
Largest dimension	mm	~104	~285
Approximate mass[1]	G	~320	N/A
Max lens diameter[1]	mm	70	N/A

Table 5.7- Draft of the optical prescription for the NFOV refractive configuration

#	Type	Radius	Thickness	Glass	Diameter
2	STANDARD	95.8996704	12.00000	CLEARTRAN	70
3	STANDARD	601.101186	9.95878		66.9936
4	BIRE__IN	-4995.23037	6.00000	AL2O3	58.0218
5	BIRE_OUT	718.445277	9.99999		54.3472
6	STANDARD	-1917.92403	12.00000	IRG26	45.7344
7	STANDARD	146.523336	6.06930		41.8258
8	STANDARD	38.3042948	8.00001	CLEARTRAN	39.0192
9	STANDARD	46.1127583	10.00000		34.4638
10	STANDARD	18.3555503	8.00001	CAF2	26.0062
11	STANDARD	12.9127278	8.53614		19.0266
12	STANDARD	26.7479626	6.00001	AMTIR1	15.419
13	STANDARD	26.008485	7.43577		11.9502
14	STANDARD	Inf	1.00000	CLEARTRAN	16
15	STANDARD	Inf	1.00000		16
16	STANDARD	Inf	0.50000	SAPPHIRE	4.864

17	STANDARD	Inf	19.10000		4.9736
18	STANDARD	Inf	0.00000		12.0014

6 NOMINAL PERFORMANCES

The quality of the image is important as well as the energy transferred by the imaging system to the image plane. Distortion is also presented here because the quality of an image is not only defined by the sharpness of the points but also by their relative position one with respect to the others.

6.1 IMAGE QUALITY

The metrics chosen to represent the nominal image quality performances of the optical configurations are the FFT MTF and the spot diagrams. The spot diagrams include only effect from geometric aberrations but the FFT MTF includes also the diffraction effects. The spot diagrams give an idea of the sharpness of the image points while the MTF gives an idea about how the contrast of any sinusoidal object patterns is reduced by the imaging process. Since any object pattern can be interpreted as a weighted sum of sinus patterns through the Fourier transform, the MTF really gives an idea about the quality of the images produced by an imaging system.

6.1.1 MTF

The MTF for the WFOV and the NFOV systems are presented in distinct sections for the clarity of the presentation.

6.1.1.1 WFOV

Figure 6.1 shows the nominal MTF for the 4 WFOV configurations presented in Section 5.1. From left to right and from top to bottom, the graphs correspond respectively to the WFOV configurations A, B, C and D. In all cases, the tangential and sagittal MTF are provided. The MTF is given at the center field and also at field angles 1.5°, 3°, 4°, 5°, 6° and at the border field located at 6.2° from the optical axis. All MTF in Figure 6.1 are computed using the Huygens method since it allows to take into account the birefringence produced by the sapphire lenses present in configurations A and B. As seen from Figure 6.1, improvements in the image quality are achieved from the configuration A to the configuration D. The configuration D is the best but configuration C is not so far.

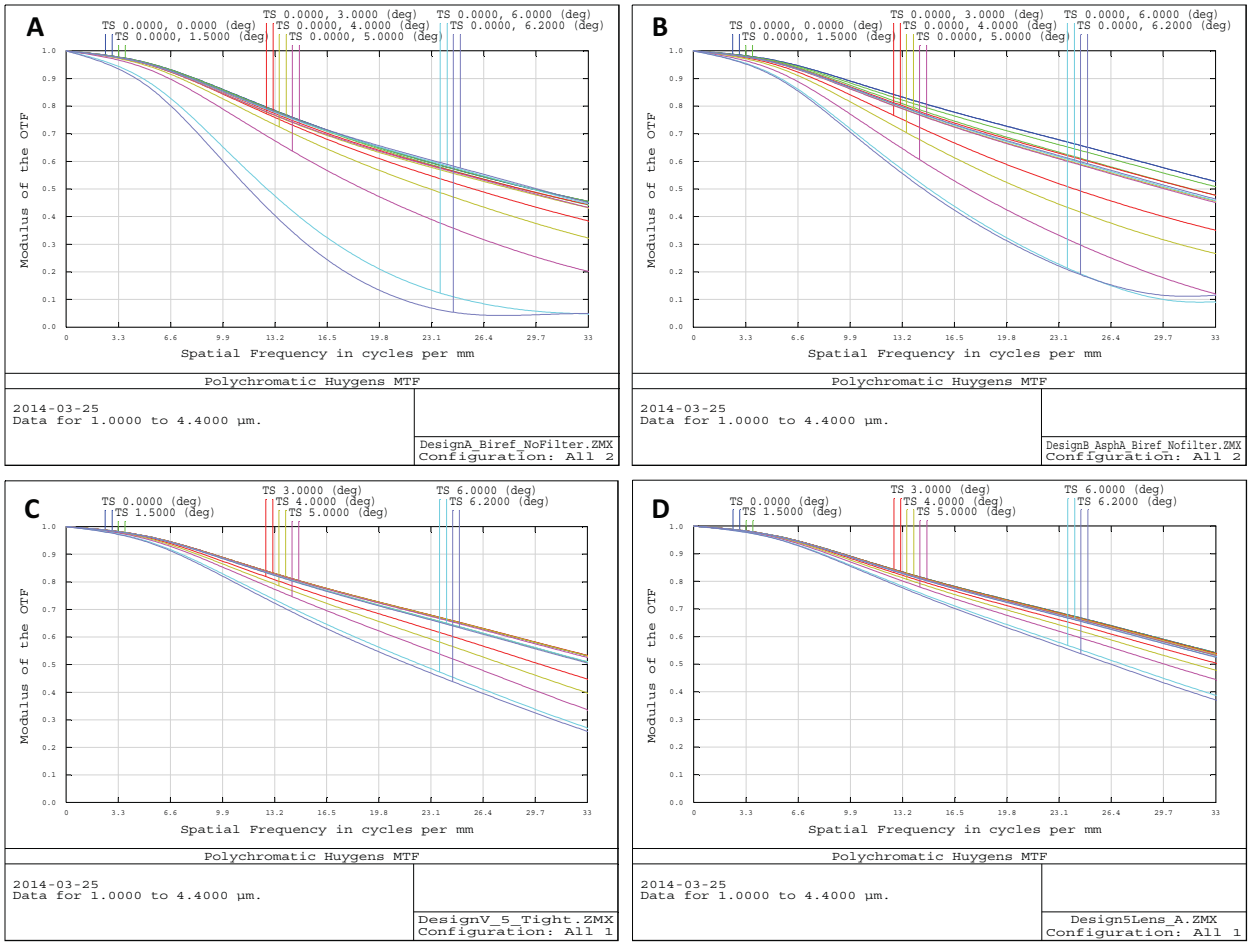

Figure 6.1- MTF for the 4 WFOV configurations of figure 5.1.

6.1.1.2 NFOV

Figure 6.2 shows the nominal MTF for the 2 NFOV configurations presented in section 5.1. From left to right, the graphs correspond respectively to the refractive and the reflective configurations. In all cases, the tangential and sagittal MTF are provided. The MTF is given at the center field and also at field angles 0.75°, 1.5°, 2°, 2.5°, 3° and at the border field located at 3.1° from the optical axis. In the case of the refractive system, the MTF are computed using the Huygens method since it allows to take into account the birefringence produced by the sapphire (AL2O3) lens included in the layout. As seen from figure 6.2, the reflective configuration is significantly superior to the refractive counterpart.

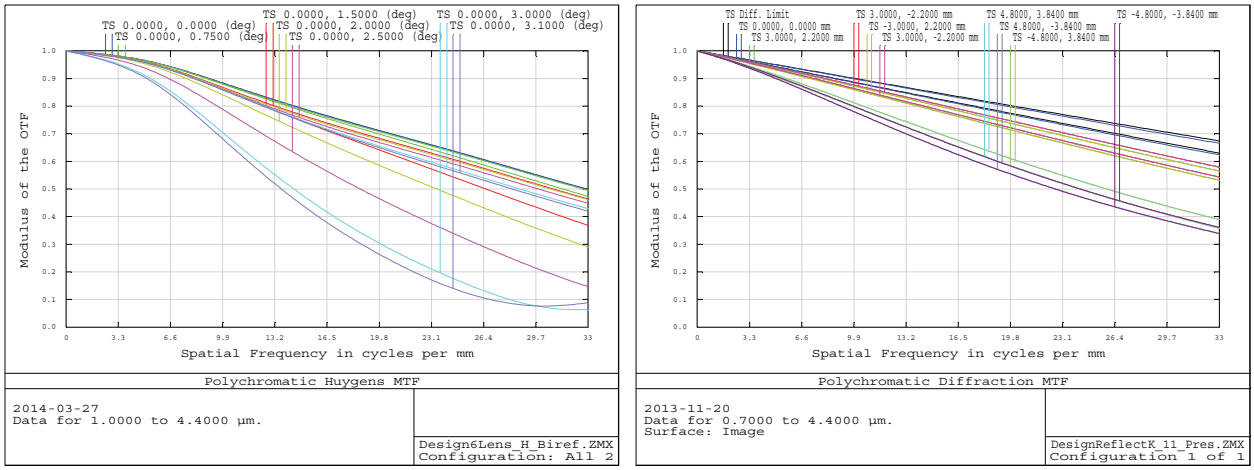

Figure 6.2- MTF for the NFOV refractive configuration (left) and the NFOV entirely reflective configuration (right)

6.1.2 Spot diagrams

As for the case of the MTF, the spot diagrams for the WFOV and the NFOV systems are presented in distinct sections for the clarity of the presentation.

6.1.2.1 WFOV

Figure 6.3 contains the spot diagrams for the 4 WFOV configurations. The spot diagrams are given at the same fields as those used for the MTF. As for the MTF, the spot diagrams reveal an increasing improvement of the image quality from configuration A up to configuration D. The spot diagrams of the configuration B are shown as green and blue dots. The green dots correspond to the ordinary rays while the blue dots correspond to the extraordinary rays as generated by the birefringence of the sapphire lens. In the other spot diagrams, the dots are colored according to their wavelength.

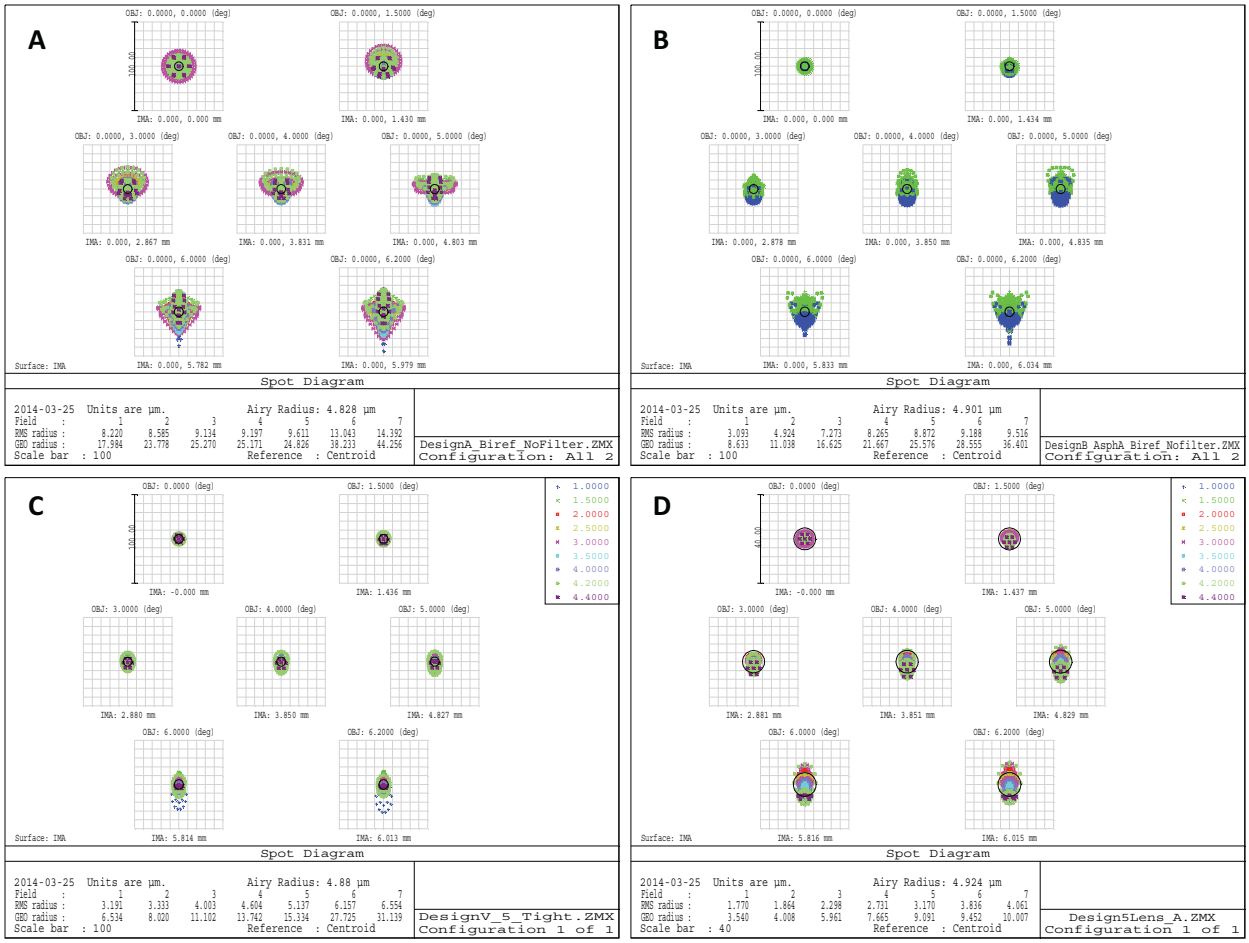

Figure 6.3- Spot diagrams for the 4 WFOV configurations.

6.1.2.2 NFOV

Figure 6.4 contains the spot diagrams for the 2 NFOV configurations. The spot diagrams are given at the same fields as those used for the MTF. As for the MTF, the spot diagrams reveal better performances in the case of the reflective configuration. The spot diagrams for the refractive configuration include contribution for both the ordinary and extraordinary rays as generated by the birefringence of the sapphire lens. The spot diagrams in the case of the reflective configuration is much better than its refractive counterpart. However, the reflective configuration is designed from the sensor plane and rays are traced in direction opposed to the normal direction (and focalized with a perfect paraxial lens). Hence, cautions are required for the interpretation of the results. Nevertheless, the reflective configuration is probably the best configuration.

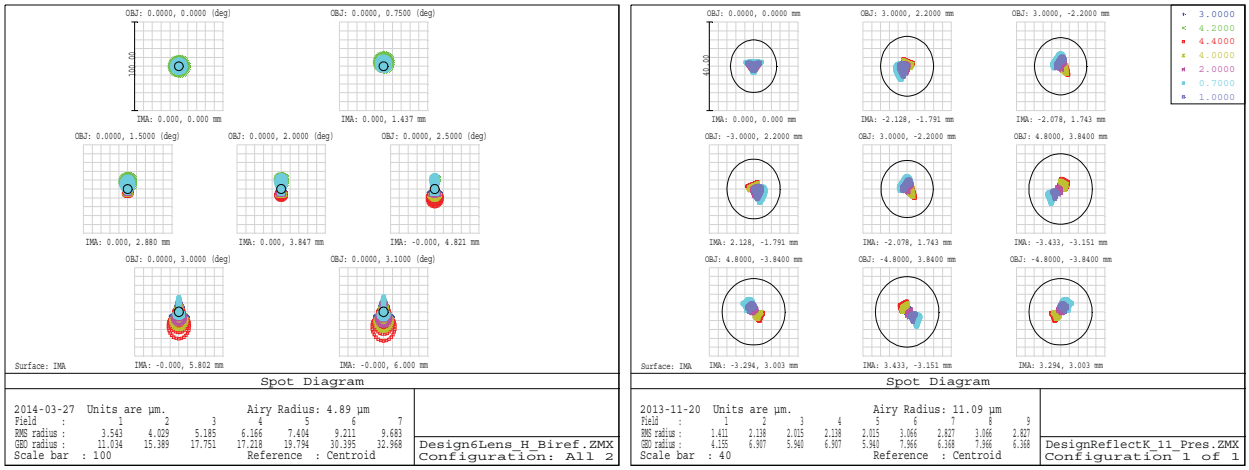

Figure 6.4- Spot diagrams for the refractive NFOV configuration (left) and the reflective configuration (right).

6.2 TRANSMISSION

The transmission of an imaging system depends on the absorption within the glasses and also on the reflection lost at the interfaces. In the case of the glass absorption, the amount of energy absorbed depends on the path length of the rays within the glass. The reflection losses at an interface depends on the angles of incidence of the rays and also on the materials and coatings at the concerned interface. In both signal reduction mechanism, the intensity of the transmitted signal is field dependent.

The optical design code can compute both the internal absorption in glasses and reflection losses at the interfaces of the nominal configurations. Data of internal absorption are normally included in the optical design code with the data on the index of refraction of the glasses. However, the material used for the design are not generally used in the 1-4.2 µm spectral band and all the data related to internal absorption have to be found, conditioned and entered in the lens design code in appropriate form.

The situation is similar for the coatings since the optical design code has the data only on simple anti-reflection coatings. The coatings recipes belong to the coating suppliers and are generally not released. A coating recipe is efficient only on a specific waveband, a range of angles of incidence and a family of glasses. Hence, various types of coatings may be required for a single optical system. The actual system operates over a large unconventional waveband and will likely require a plurality of custom coatings. Considering the time frame allowed for the study, only theoretical coatings with uniform properties over the angles of incidence and wavelengths were considered. In this perspective, idealized coatings with 1% reflection losses per optical interface have been simulated on all of the optical surfaces in all the refractive configurations. The energy transfer has been computed only for the refractive configurations and the transmission maps appears in figure 6.5 for the WFOV cases and figure 6.6 for the NFOV refractive configuration.

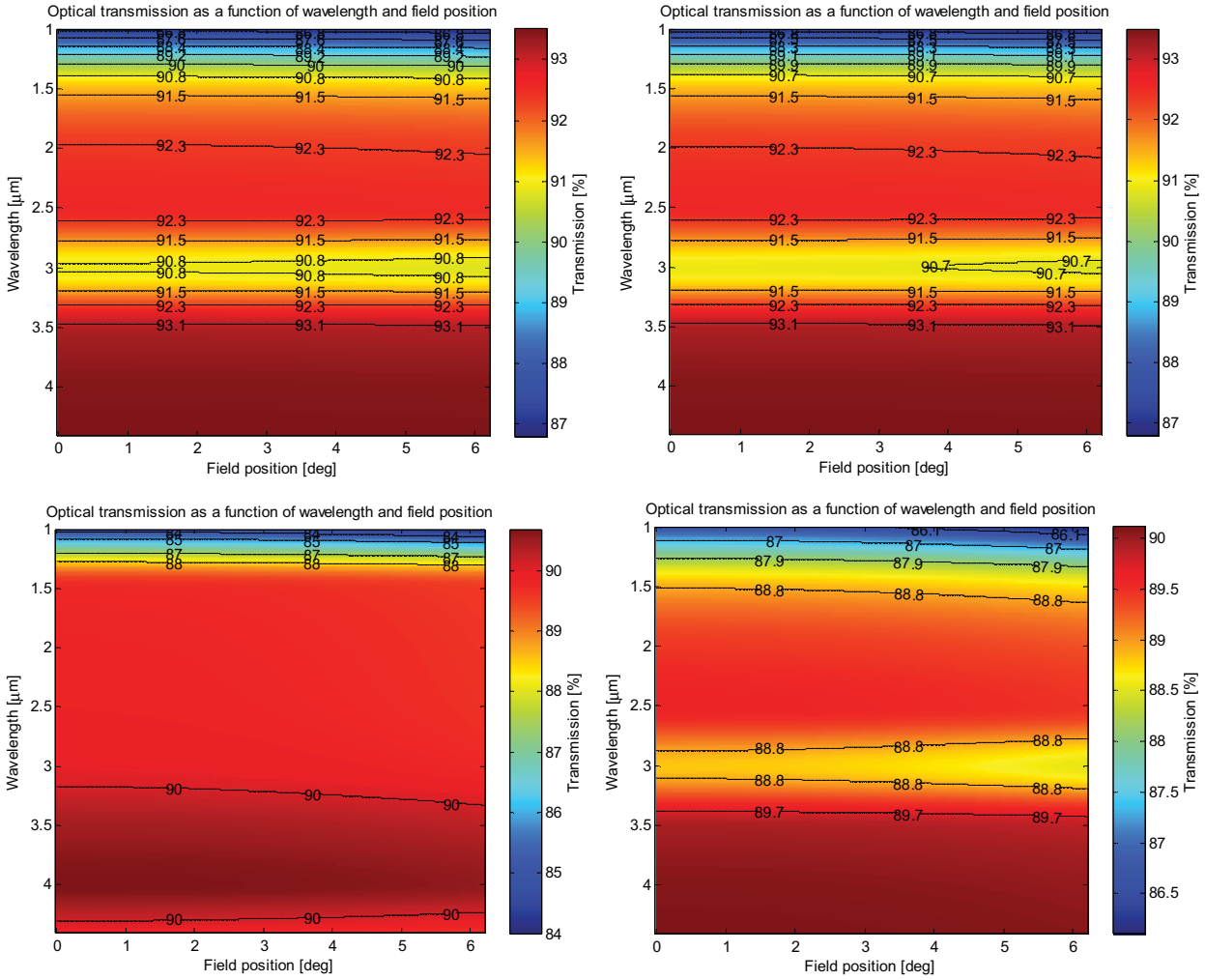

Figure 6.5- Optical transmission maps as a function of the wavelength and field position for WFOV configurations A, B, C and D respectively in the usual order.

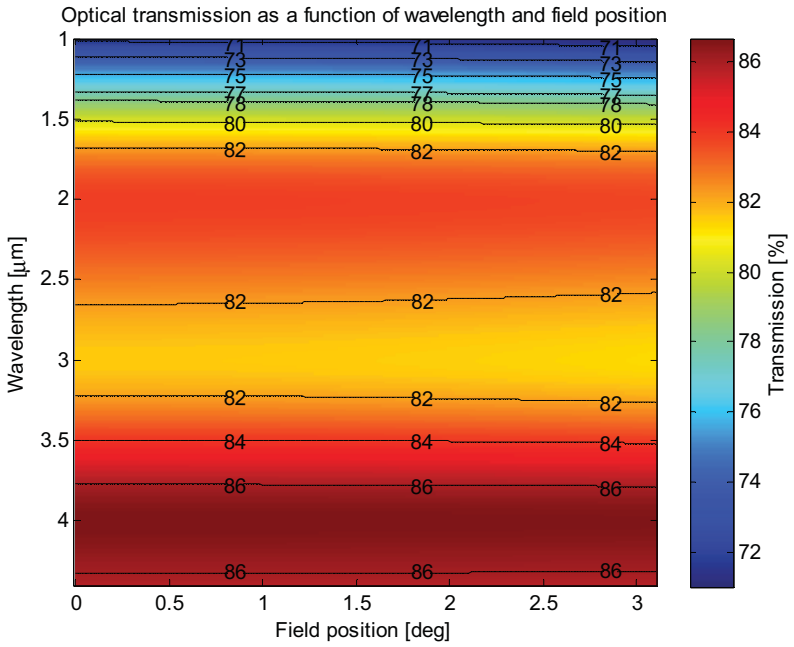

Figure 6.6- Optical transmission maps as a function of the wavelength and field position for NFOV refractive configuration.

6.3 DISTORTION

Distortion is an alteration of the original object shapes. The distortions are caused by variations in the magnification factor according to the field position. Constraints have been imposed during the design process in order to maintain the distortion below 1%.

Figure 6.7 shows the level of nominal distortion computed for the 4 WFOV configurations while figure 6.8 show the distortion for the two NFOV nominal configurations. The objective of maintaining the distortion below the 1% level is pretty much achieved for the refractive configurations but not for the NFOV reflective configuration. Again, the NFOV reflective configuration was only at an early development stage and caution must be taken in the interpretation of the distortion. A trapezoidal schema is clearly seen on the grid distortion graph and this is not surprising since the mirrors are tilted and used in off-axis mode. The trapezoidal schema is responsible for most of the distortion in the case of the reflective NFOV configuration and this effect can probably be reduced.

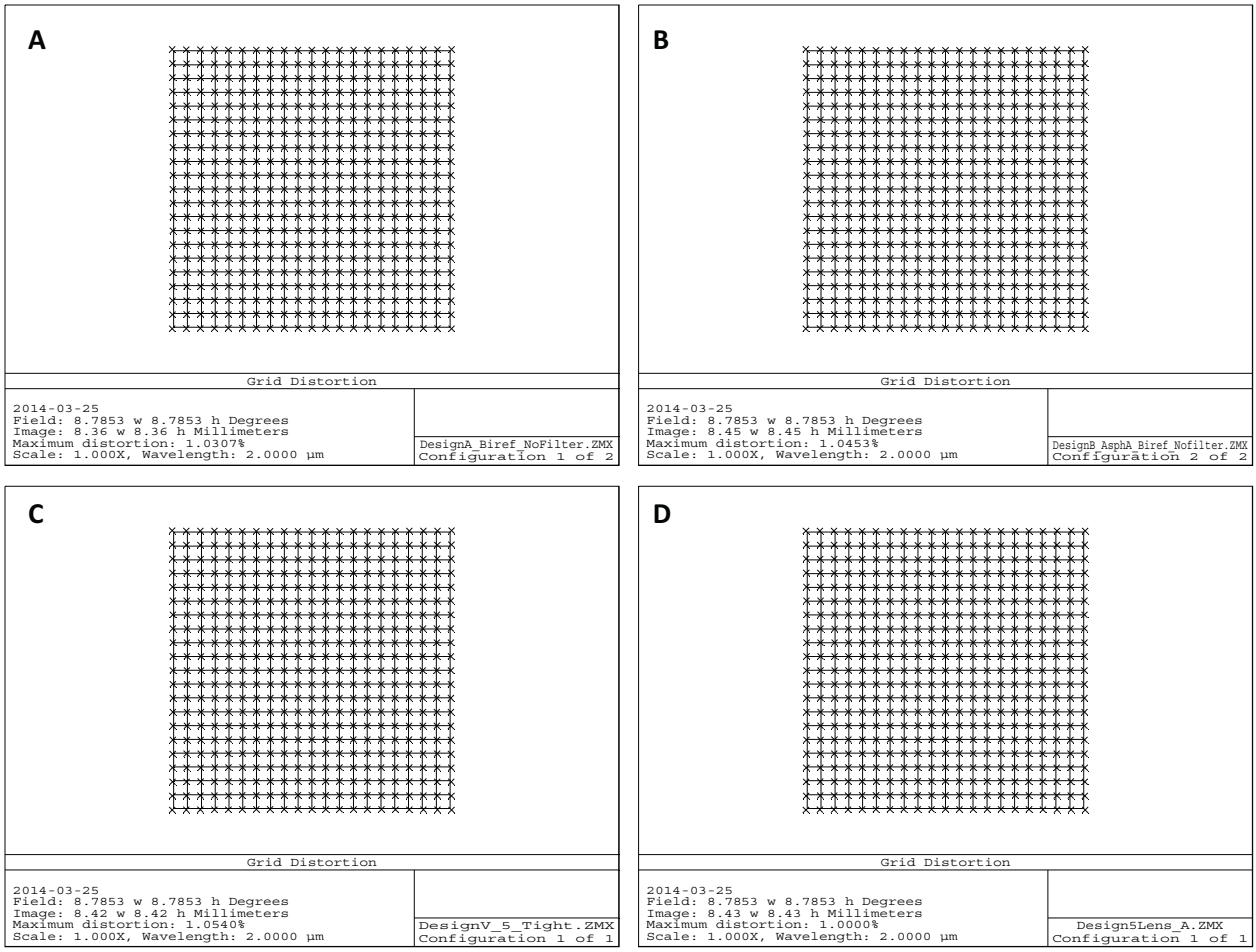

Figure 6.7- Distortion for the 4 WFOV configurations.

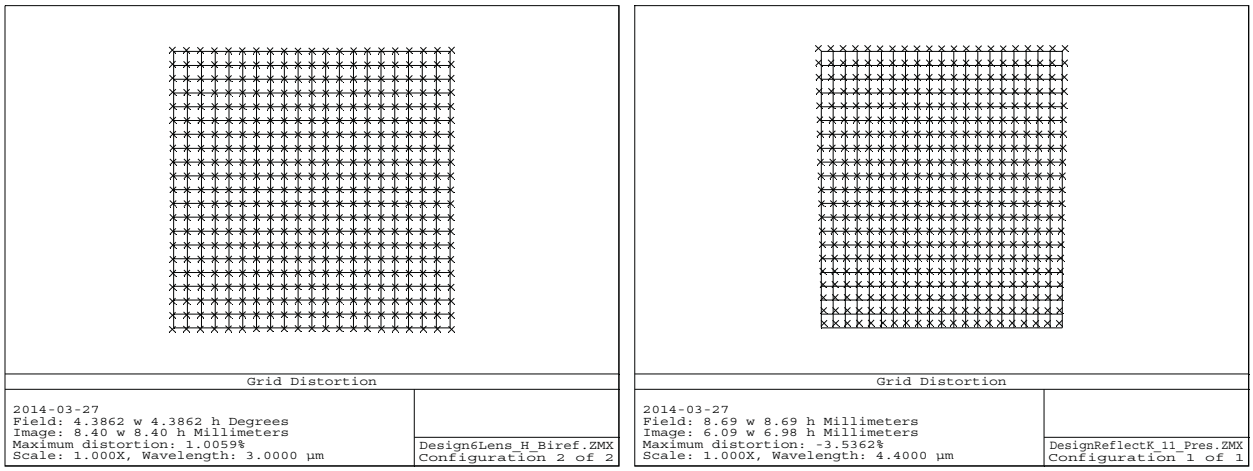

Figure 6.8- Distortion for the 2 NFOV configurations. The trapezoidal distortion is clearly seen on the grid distortion (right) corresponding to the reflective configuration.

7 THERMAL BEHAVIOR

The refractive indices of the material as well as the shape of the lenses and their mechanical supports change with temperature. Hence, some amount of degradation of the optical performances are expected at operational temperatures different from the nominal temperature. Mechanisms either passive or active can be considered to minimize the degradation caused by temperature changes. Before considering some form of thermal compensation, a thermal analysis must be done to verify if a compensation mechanism is required. In this perspective, a simple preliminary thermal analysis was conducted on the all-spherical 4 lenses WFOV configuration C. The hypothesis considered for this study are listed in table 7.1 below.

Tables 7.1 – Hypothesis used for the thermal analysis

	Hypothesis	Comments
Temperature range	-40°C to 50°C	Corresponds to the operational temperature
Nominal temperature	20°C	Temperature considered during the assembly of the system.
Compensator	None	No passive or active mechanism considered. Only a refocus by the user is considered.
Mechanical supports	Aluminum	All the mechanical supports are considered to be made of aluminum with a unique linear thermal coefficient of expansion 23.6 x 10^{-6}/°C valid for the entire range of temperature.
Temperature gradients	None	It is considered that the system is used only when it is thermally stabilized and that all thermal gradients both in the optical and the mechanical elements have been reduced to negligible values.
Object distance	Infinity	In all simulation performed for the thermal analysis, the object was considered to be located at an infinite distance from the system. For object located at infinity, a field is located with the angle it subtend with respect to the system's optical axis.

The main results obtained in the thermal analysis are displayed in figure 7.1 for three fields, i.e. the center and the border field (6.2) and a field (4°) in between the center and the border. The performances are presented through the FFT MTF corresponding to the mean between the tangential and the sagittal values. The MTF value is given by the color of the points on the map and the correspondence between the colors and the MTF values (in %) is reported through the color bar located on the right side of the map. The MTF is mapped as a function of the spatial frequency in abscissa and of the temperature in ordinate. Very little variations with the temperature is observed on all the MTF maps, meaning that temperatures changes from the nominal value translate mainly in defocus that can be corrected with a refocus.

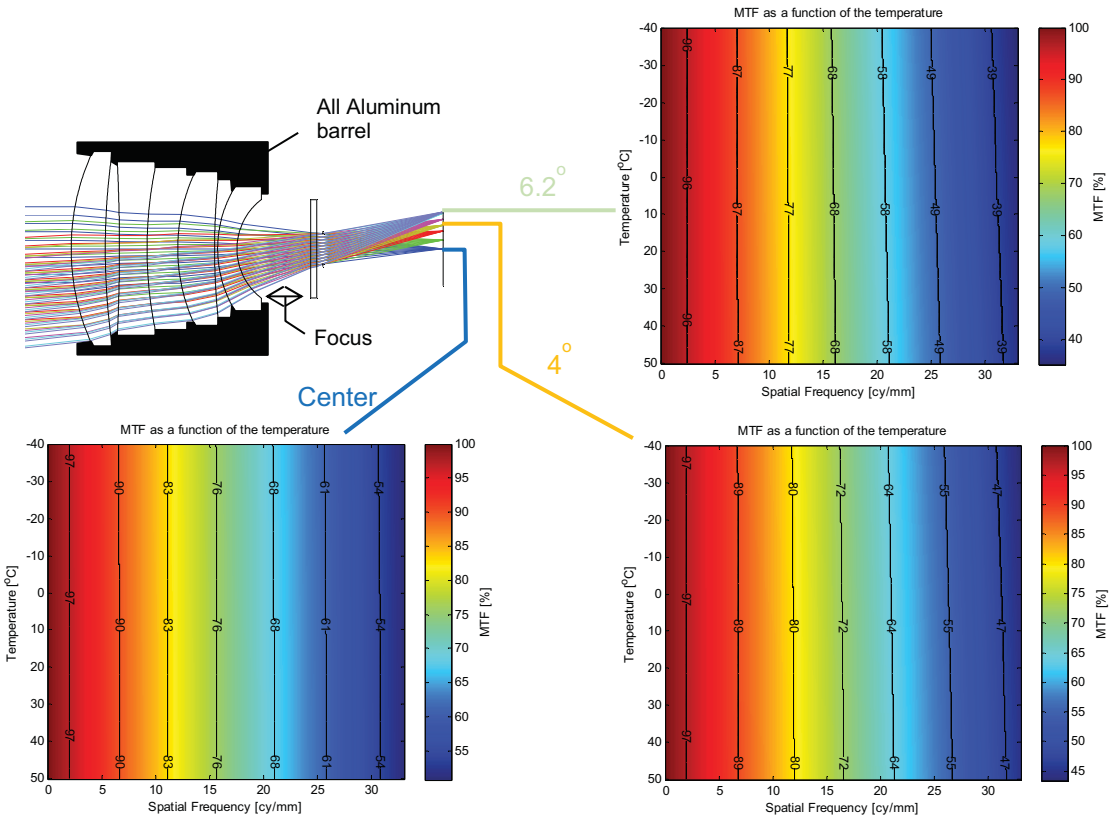

Figure 7.1- FFT MTF for configuration C at different temperatures for three fields. The mean on tangential and sagittal value is given on all the MTF maps.

8 PRELIMINARY PARASITIC LIGHT ANALYSIS

The anti-reflection coatings applied on the optical surfaces are not perfect and a certain part of the energy of an incident ray is transmitted through the interface but a small amount is reflected. Thus each ray is divided into a transmitted ray and a reflected ray at each of the interface. In a refractive optical system, the rays reflected on the interfaces represent not only signal losses but can also become noise on the image. Noise or parasitic light arises when some reflected rays are returned toward the image plane through a series of reflections. Fortunately, the energy of a parasitic ray decreases rapidly with the number of reflections. The worst scenario happens when the parasitic rays are focused close to the image plane after only two reflections. Images of the scene can be produced by the parasitic rays through a succession of transmissions and reflections. Such ghost images can be generated through complex transmission/reflection schemes involving two, three or more reflections. Such ghost image might introduce disturbing artifacts for the observer.

General parasitic light analysis can be performed through non-sequential ray tracing. In conventional ray tracing, the rays are traced in a predefined sequence according to the order of appearance of the optical surfaces in the definition list. In the conventional mode, a ray is either transmitted or reflected according to the chosen definition parameters. In non-sequential ray tracing, the optical components

are defined as 3D elements with optical properties for each of its surfaces. Each ray is traced up to the next element encountered by its trajectory. At each intersect of a ray with an optical element, the ray is split into its refracted and reflected components with the energy distribution computed according to the Fresnel model. The process continues for each of the two rays thus generated until the next elements encountered by those rays and so on. In this manner, a single parent ray launch from a source is rapidly splits in many generations of child rays. The non-sequential ray tracing allows the simulation of the complex distribution of the optical energy within an optical system in a quite realistic manner. It is a very powerful tool for parasitic light analysis.

A non-sequential model has been generated for the analysis of the parasitic light in the case of the WFOV configuration C. The model is shown on figure 8.1 with the child rays issued from a single parent ray. In the model, the parent rays are launched from a circular surface located just in front of the first optical surface. The launch point of a parent ray is randomly chosen according to a uniform distribution and it direction is also chosen randomly (uniform distribution) within a cone with apex angle corresponding the total field of view of the objective lens. This simulates approximately the rays produced by a distant scene with uniform intensity and dimensions covering the entire field of view of the objective lens. A detection element is added in the model at the exact position foreseen for real pixel array. This detection element has the same dimensions of the Kinglet's sensitive surface.

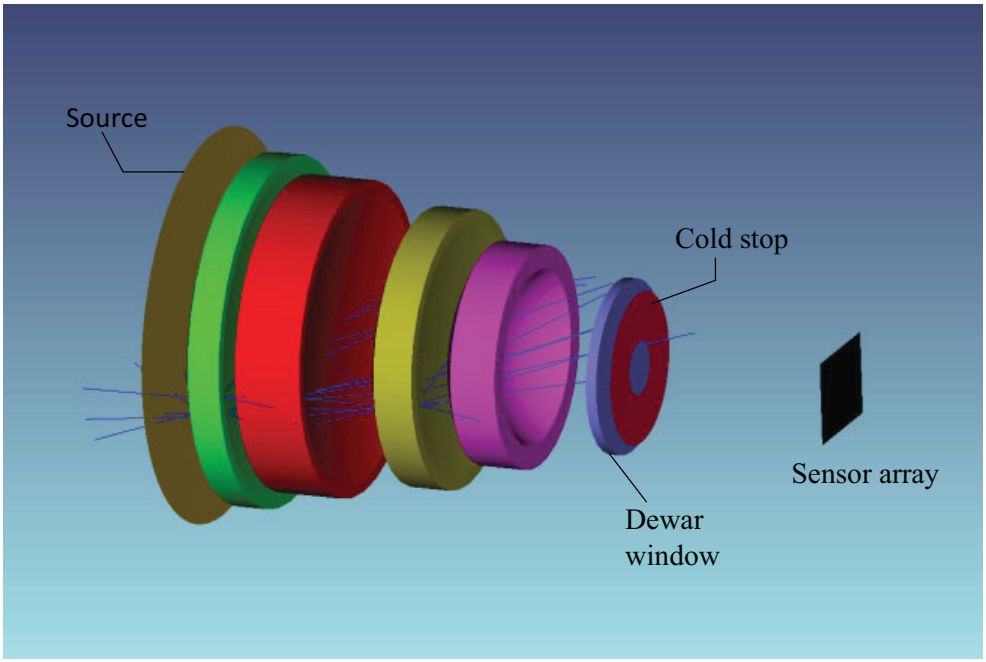

Figure 8.1- Non-sequential model of the WFOV configuration C.

Figure 8.2 shows the results of the non-sequential ray tracing using the model described in figure 8.1 above. A total of 10 million parent rays were launched to obtain the results presented in figure 8.2. The leftmost image corresponds to the intensity received by the detector element when all the rays are considered. The rightmost image corresponds to the intensity distribution on the detector produced by the parasitic rays. This distribution was obtained by filtering out the direct rays. The case where all the rays are considered corresponds approximately to the image that would be obtained with the optical

system for a uniformly illuminated scene. Except for discretization noise, the intensity distribution is quite uniform as expected. Note that the four corners of the intensity map are not illuminated because the span angle of the rays was just a bit smaller than the effective angular field of view of the system. The intensity distribution associated with the parasitic rays (right) decreases progressively with increasing distance from the center. This is not surprising because the parasitic rays are subject to be vignetted by the finite dimensions of the lenses. The non-uniform intensity distribution can also be caused by focusing of the parasite rays at more or less distant position in front or behind the detector plane. The most significant data obtained from the two intensity maps is the total optical power received by the detector. According to the rightmost intensity map, the total parasitic light reaching the detector is about 3.65×10^{-5} Watt while the total optical power received by the detector is about 0.0816 Watt when all the rays are considered (useful optical signal plus the parasitic light). This involves that the useful optical signal is 2000 times higher than the optical noise.

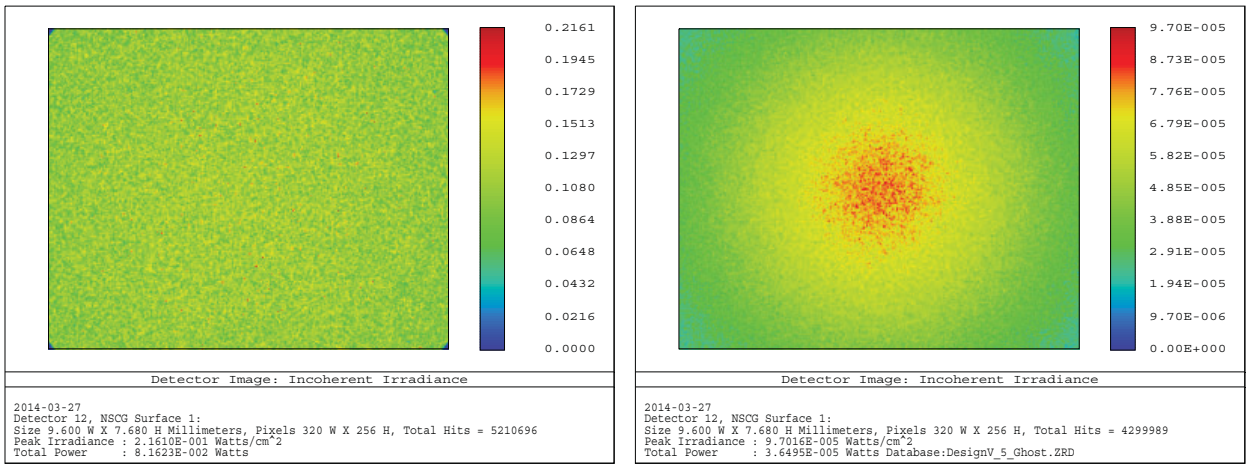

Figure 8.2- Intensity distribution on the detector. All rays are considered for the case on the left while only parasitic rays are considered on the right.

9 FURTHER DEVELOPMENT

Significant work have been done during the optical design of the objective lens. However, further improvements, analysis, simulations and evaluations still remain to be performed before the realization of a prototype. Table 9.1 gives a non-exhaustive list of main steps/tasks to be done in order to pursue further the development.

Table 9.1-Steps/Tasks for the realization of a prototype.

#	Steps/Tasks	Comments
1	Improvement of the designs	Interesting designs were obtained in the case of the WFOV. The configuration C seems to be a good compromise between the performances and complexity. Another optimization cycle might provide improvement on the compactness, mass and transmission. The chalcogenide glasses present a bit of internal absorption and it would be beneficial to try to reduce the path length inside the material. It would also be interesting to try to reduce the length of the objective lens.

		In the actual study, conventional approaches were considered. The addition of a diffractive surface for the control of the chromatism offers interesting perspective for the reduction of the number of element and the mass. This is especially interesting with chalcogenide elements since the diffractive surface can be included to the lens in a single molding operation. This approaches may be interesting for reduction of the mass in the case of the NFOV configuration.
2	Complete tolerances analysis	No tolerance analysis has been performed in this study. A complete tolerance analysis is required to determine the level of precision required for the manufacturing of the optical elements and their alignment into the system.
3	Opto-mechanical design with complete tolerances analysis	The level of precision for the positioning of the optical element depends on the way those elements are linked with their mechanical supports. A tolerance analysis is not complete without the integration of the mounting approaches. Some tolerance concerns only the optical manufacturing but others depends also on mechanical parameters while others (air space) depends only on the mechanical design. A complete tolerance analysis must also include the budget for the tolerances shared by the optical manufacturing, the mechanical design and manufacturing.
4	Elaborate thermal analysis	A preliminary thermal analysis has been performed in this study. According to this analysis, the WFOV configuration C seems to tolerate temperature variation without affecting significantly its optical performances. A more precise and complete analysis is required to confirm the main conclusion of the preliminary analysis.
5	Parasitic light analysis	A simple preliminary parasitic light analysis was performed in this study and revealed no major problem at least in the case of the WFOV configuration C. A more complete analysis that includes parasitic reflections on mechanical supports (to be designed) is needed before drawing definitive conclusions on stray light.
6	Procurement process cycle	The main uncertainties for the procurement of the optical elements concern the anti-reflection coatings and the chalcogenide materials. It is to be verified that Canadian manufacturers can have access to the chalcogenide raw material. Custom design coatings will likely be required for the actual objective lens. The coatings can be provided by US suppliers, Canadian supplier will have to be searched for. The Canadian manufacturers can probably produce the spherical lenses of the WFOV configurations. However, there are concerns about toxicity of the materials and the availability of the protection equipment. Some further work on the procurement must be done.
7	Assembly procedure	The assembly procedure consists in listing all the steps required for generating a functional unit. It includes the identification of the critical or challenging operations together with the approaches to overcome the difficulties related with them. Also included in the procedure is the identification of the devices or apparatus that should be used for assisting the technologist during processes and adjustments or for the evaluation of metrics attesting the level of success of those processes, adjustments or operations.

10 SYNTHESIS & CONCLUSION

This design study was originally motivated by the recent apparition of new sensors with unconventional sensitivity spectral band covering the NIR up to nearly MWIR upper limit. More specifically, the design study was oriented in function to the Kinglet sensor developed by SCD of Isreal. The study consisted in the draft optical design of two types of imaging configurations operating in the 1-4.2 µm wide spectral band, namely a version with a 4x5° narrow field-of-view (FOV) and its wide FOV counterpart with 8x10° total angular field-of-view.

The study allowed the generation of interesting preliminary refractive configurations in the case of the WFOV version. Compact and lightweight optical layouts were obtained through the use of crystal materials commonly used in MWIR and LWIR optics and special (chalcogenide) glasses transmitting from the NIR up to the LWIR. An interesting refractive layout for the NFOV version was obtained but this layout includes more than 300 g of optical material and was considered too heavy for the foreseen applications. For the NFOV version, an entirely reflective configuration was also designed but it was not considered interesting due to its large size. Table 10.1 lists the basic characteristics of the preferred WFOV configuration and also for the NFOV refractive configuration. Both configurations consists on spherical surfaces only, which maximize the chances for a production in Canada. Both the two configurations include chalcogenide glasses for which the raw materials procurement of can be difficult from Canadian lens manufacturers. Nevertheless chalcogenide glasses are also available outside USA [7]. Improvement in the availability of the chalcogenide is expected in the future [7] [2].

Table 10.1- Basic characteristics of the preferred WFOV and the refractive NFOV configurations

Characteristic	WFOV	NFOV
Field-of-view (FOV)	8°x10°	4°x5°
Image size	7.68 mm x 9.6 mm	7.68 mm x 9.6 mm
F/#	4	4
Focal length	55 mm	110 mm
Number of lenses	4	6
Approximate maximum lens diameter[1]	30 mm	70 mm
Total length up to Dewar window	39 mm	104 mm
Clear distance, last surface/Dewar window	9.1 mm	6.7 mm
Focus range	25 m to ∞	25 m to ∞
Spectral range	1-4.4 µm	1-4.4 µm
Operational thermal range	-40 to 50 °C	-40 to 50 °C
Approximate mass for the optical material[1]	43 g	320 g
Max distortion	~1%	~1%

1- Tight diameters. Diameters allowing all the rays to be transmitted. No extra space added for the contact with the mechanical supports

Preliminary thermal and parasitic light analysis have been performed in the actual study on the preferred WFOV configuration. No significant problem has been revealed by these analysis. However, they were preliminary analysis and more complete analysis are required in a next phase. This analysis should include the effects of the mechanical supports (still to be designed).

Conventional design approaches were considered for this study. It would be interesting to investigate the possibility to include diffractive surface for the chromatism control and also for reduction of the number of elements, the mass and volume of the optical system. Nevertheless, it has to be kept in mind that this avenue involves significant efforts for the design and analysis as well as for the manufacturing.

REFERENCES

1-Hewak, D. W., 'Chalcogenide glasses for photonics device applications'. http://www.orc.soton.ac.uk/viewpublication.html?pid=4996

2- http://www.flir.com/flirone/explore/#slide-4

3- Schott glass IRGxx data sheets: http://www.us.schott.com/advanced_optics/english/products/optical-materials/ir-materials/infrared-chalcogenide-glasses/index.html

4- http://www.stingrayoptics.com/superband-series

5- Klipstein, P. C. et al, 'LowSWaP MWIR detector based on XBn Focal Plane Array',

6-Nathan Carlie,'Chalcogenide custom glass development'. PowerPoint presentation. See: http://spie.org/Documents/Industry%20relations/IR%20standards%20working%20group/Carlie%20Technical%20DSS-2012.pdf

7- Guimond, Y. & Y. Bellec, 'Molded GASIR infrared optics for automotive applications', Proc. Of SPIE Vol. 6206, 62062L (2006)

8- Cleartran data sheet: http://www.lightmachinery.com/Materials/cleartran.pdf

9- ZnSe data sheet:

http://www.dow.com/assets/attachments/business/gt/infrared_materials/cvd_zinc_selenide/tds/cvd_zinc_selenide.pdf

10- Calcium fluoride data sheet from Corning: http://www.lightmachinery.com/Materials/H0607_CaF2_Product_Sheet.pdf